Peer reviewed version

Link to published version (if available):
10.1146/annurev-conmatphys-032922-094430

Link to publication record in Explore Bristol Research
PDF-document

University of Bristol - Explore Bristol Research
General rights

Charge correlations in cuprate superconductors

Stephen M. Hayden[1] and John M. Tranquada[2]

[1]H. H. Wills Physics Laboratory, University of Bristol, Bristol, United Kingdom, BS8 1TL; email: s.hayden@bristol.ac.uk
[2]Condensed Matter Physics and Materials Science Division, Brookhaven National Laboratory, Upton, NY, USA, 11973-5000

Abstract

High-temperature superconductivity, with transition temperatures up to ≈134 K at ambient pressure, occurs in layered cuprate compounds. The conducting CuO_2 planes, which are universally present, are responsible for the superconductivity, but also show a disposition to other competing states including spin and charge order. Charge-density-wave (CDW) order appears to be a universal property of cuprate superconductors. It has been studied via a multitude of probes including x-ray and neutron scattering, nuclear magnetic resonance, scanning probe techniques, electronic transport and quantum oscillations. Here we review the microscopic properties of the CDW order. We discuss the nature of the ordered state, that is, its symmetry and microscopic structure. Further we show how the CDW order is related to quenched disorder, host structure, symmetry breaking perturbations and magnetic fields. We also describe measurements of dynamic collective charge excitations which are closely related to the quasi-static CDW order. Finally, we highlight some of the debated issues in the field including, the origin of the CDW order, the relationship to spin order and nature of the spatial CDW correlations.

1. INTRODUCTION

The investigation of cuprate superconductors over the last four decades has been characterized by reports of various ordered states in addition to the superconductivity (SC). These states are frequently presented in a phase diagram as a function of doped-hole concentration, p, and temperature, T (1). There one can see that the superconducting transition T_c has a dome-like shape that rises from a neighboring antiferromagnetic (AF) insulator state at $p \sim 0$ and drops towards zero at $p \sim 0.3$, where a metallic phase takes over. The maximum T_c occurs at $p_{\mathrm{opt}} \approx 0.16$. Between the AF regime and just beyond the peak of the dome, it is common to draw a line $T^\star(p)$, starting at a $T^\star$ of several hundred K for small p and decreasing toward the dome peak, representing the onset of a "pseudogap" state. Within the pseudogap regime, electronic states gradually develop coherence on cooling, but only on parts of the nominal Fermi surface (2).

Charge-density-wave (CDW) correlations represent one type of "order" that has been experimentally observed in many cuprate families, with the strongest order occurring near $p = 1/8$. The doping and family dependent onset temperatures fall below $T^\star$, so that CDW correlations cannot be the explanation of the pseudogap. At the same time, it is relevant to note that the optimum ordering temperatures associated with superconducting, CDW (T_{CDW}) and magnetic (Néel temperature, T_{N} of the AF parent phase) orders are comparable, with $T_c \approx 140$ K, $T_{\mathrm{CDW}} \approx 150$ K and $T_N \approx 300$ K. Thus, the cuprate superconductors have fascinating, finely-balanced competing and intertwined phases (3). Here we will focus on experimental aspects of CDW correlations and related charge excitations in hole-doped cuprates.

1.1. Probing charge density waves

CDW order is a fairly common phenomenon in metallic compounds that are layered, such as $NbSe_2$ and $TaSe_2$ (4), or quasi one dimensional (1D) such as $NbSe_3$ and $(TMTSF)_2PF_6$ (5), where the valence charge becomes periodically modulated, with an associated displacement pattern of the atomic lattice. In the 1D case, the CDW order can be driven by purely electronic energies. In the 2D case, however, it has been argued that strong electron-phonon coupling is essential (6). **Figure 1a** illustrates the charge correlations in a metal: charge density fluctuations disperse out of the wave vector $\mathbf{q}_{\mathrm{CDW}}$ characteristic of CDW order.

At a different extreme, there are also layered Mott insulators, isostructural with superconducting $La_{2-x}Sr_xCuO_4$ but with Cu replaced by Ni, Co, or Mn that develop CDW order intertwined with antiferromagnetic spin-density-wave (SDW) order when doped (7). To distinguish these from the more conventional case, the modulated states have been referred to as "stripe orders." However, the order parameter for the charge modulation (and atomic displacements) is the same as for the metallic case, so we will use CDW as a generic descriptor.

X-ray and neutron diffraction are commonly used to detect CDW order, through their sensitivity to the associated lattice modulation. Diffraction from single crystals performed on spectrometers that analyze the incident and scattered wave vectors using neutrons or hard x-rays can typically achieve an energy resolution of ~ 1 meV, smaller than most relevant excitations, though not smaller than glassy fluctuations. Sensitivity to element-specific contributions to charge order is obtained with resonant x-ray scattering (RXS) (8). When the the scattered photons are energy resolved, the technique is known as resonant inelastic

AF: antiferromagnet

CDW: charge-density wave

SDW: spin-density wave

XS: x-ray scattering

IXS: inelastic x-ray scattering

RXS: resonant x-ray scattering

RIXS: resonant inelastic x-ray scattering

NS: neutron scattering

SI-STM: spectroscopic imaging scanning tunneling microscopy

NMR: nuclear magnetic resonance

x-ray scattering (RIXS). With RIXS, one can resolve elastic scattering from collective excitations. The state of the art for energy resolution in the soft x-ray regime, most relevant to cuprates, is ~ 20 meV.

CDW order can be imaged in real space with scanning tunneling microscopy (STM), where well-ordered modulations of atomic positions can be detected at the surface of a compound such as $NbSe_2$ by topographic imaging (9), whereas spectroscopic imaging (SI-STM) probes the spatial modulation of the local density of electronic states in energy (10).

Another technique that provides local information, but in this case without restriction to the sample surface, is nuclear magnetic resonance (NMR) spectroscopy. NMR is sensitive both to the hyperfine magnetic field from atomic moments and to charge correlations through electric field gradients (11). NMR spectroscopy typically requires application of a strong magnetic field, which must be taken into account when comparing with other measurements. At the same time, the resonance frequencies used tend to be in the MHz (μeV) range, so that NMR is an effective tool for distinguishing between static and dynamic behavior.
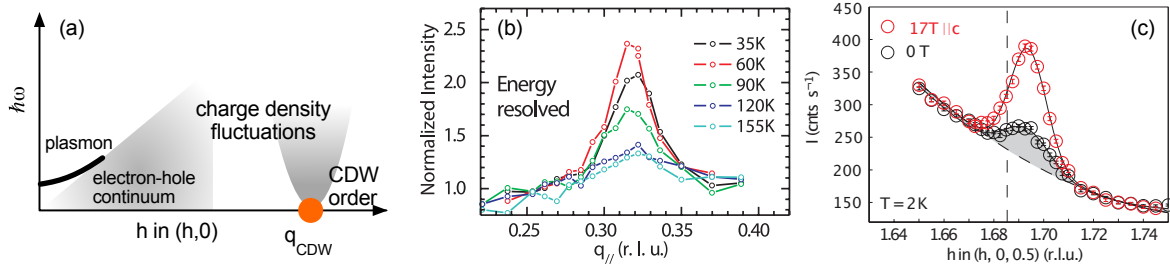

Figure 1

Charge order and collective charge excitations in cuprates. (a) Schematic of the energy and wavevector dependence of the collective charge excitations. At small h acoustic plasmons and the electron-hole continuum are observed. A quasi-static charge ordering peak is observed at $\mathbf{q}_{CDW}$ centered on $\hbar\omega = 0$. Dispersing charge excitations are observed at near $\mathbf{q}_{CDW}$. (b-c) The charge ordering peak in YBCO ($p \approx 0.12$) observed by (b) Cu L-edge RIXS (12) and (c) hard (100 keV) x-ray scattering (13). (b) reproduced with permission from Ref. (12) and (c) reproduced with permission from (13).

1.2. Discoveries of charge density waves in cuprates

Early evidence for CDW order in cuprates came from a neutron scattering study of the $La_{1.6-x}Nd_{0.4}Sr_xCuO_4$ (Nd-LSCO) system at $p = x = 0.12$, a composition at which bulk superconducting order is strongly suppressed (14). SDW order, with twice the $\sim 4a$ period of the CDW, appeared at a lower temperature. While the CuO_2 layers common to cuprates are often assumed to have a square lattice, the low-temperature structure of Nd-LSCO has broken rotational symmetry in the planes, which led to the inference that the CDW in each layer is modulated in only one direction, which we label as a 1-$\mathbf{q}$ CDW. A RXS study of the CDW on the closely related compound $La_{2-x}Ba_xCuO_4$ with $x = 1/8$, probing the O-K and Cu-L_3 edges, demonstrated that the doped holes in O $2p$ orbitals are spatially modulated and that there is also a response involving the Cu $3d$ holes (15).

Evidence for related electronic modulations also came from SI-STM on a different cuprate. STM requires an atomically flat surface, so cleavable $Bi_2Sr_2CaCu_2O_{8+y}$ (Bi2212)

LBCO:
$La_{2-x}Ba_xSr_xCuO_4$

LSCO:
$La_{2-x}Sr_xSr_xCuO_4$

Nd-LSCO:
$La_{1.6-x}Nd_{0.4}Sr_xCuO_4$

YBCO:
$YBa_2Cu_3O_{6+x}$

Bi2212:
$Bi_2Sr_2CaCu_2O_{8+x}$

Hg1201:
$HgBa_2CuO_{4+y}$

Tl2201:
$Tl_2Ba_2CuO_{6+\delta}$

was the target of choice. It was found that in the superconducting state the application of a magnetic field, which is screened in the bulk by quantized superconducting vortices, induces a checkerboard-like 2-$\mathbf{q}$ electronic modulation in a "halo" region about each vortex core with a period of $\sim 4a$ (16). Another group noted the presence of similar modulations in zero magnetic field (17).

Another much-studied cuprate is $YBa_2Cu_3O_{6+x}$ (YBCO). Measurements of transport properties, such as the Hall effect, on an underdoped crystal in very high magnetic fields revealed quantum oscillations indicating the presence of small Fermi-surface pockets (18). This observation motivated proposals that the pockets might be the consequence of a density wave such as CDW order (19, 20). Direct evidence for CDW order came from high-field NMR measurements on YBCO ($p = 0.108$) (21) where it was found that charge ordering onsets at $T \approx 60$ K (comparable to the zero-field T_c) in magnetic fields of 28.5 T, and with the absence of any SDW order. Resonant (12) and non-resonant (13) x-ray measurements found diffraction evidence for charge order in superconducting YBCO, as illustrated in **Figure 1b-c**, with dopings similar to the NMR sample. In contrast to the NMR results, the CDW signal was found to appear at a temperature far above T_c, and to decrease below T_c.

This cursory historical description indicates a number of puzzles and apparent inconsistencies. Is there evidence of true long-range order as one would expect for a thermodynamic phase of matter? What is the significance of evidence that the CDWs are sometimes 1-$\mathbf{q}$ and other times 2-$\mathbf{q}$ correlations? How is the CDW correlated between CuO_2 planes? Are there "static" and "dynamic" components to the CDW correlations? What structural features of lattice order or disorder impact the appearance of CDW correlations? What is the relationship between CDW correlations and superconductivity, and how is this impacted by an applied magnetic field? What do the atomic displacement patterns associated with a CDW look like? What is the relationship between CDWs, SDWs, and fluctuating spin correlations? What are the implications of the studies of quantum oscillations and Fermi surface reconstruction?

In the following, we attempt to address these questions and identify systematic behaviors underlying the experimental observations. We then give a very brief mention of theoretical perspectives, before summarizing and identifying open questions.

2. Nature of the charge correlations in cuprates

In a conventional continuous (second-order) phase transition, one expects to observe critical (dynamic) fluctuations of the order parameter whose correlation length ξ diverges on cooling to the transition temperature. Below the transition, the order parameter is finite and a static correlation extends across the entire system (i.e. $\xi \to \infty$), with growth of the order parameter on cooling below the transition. In cuprates, the CDW correlations never follow this behavior. The fundamental reason for this is that cuprates are not clean homogeneous systems with simple crystal structures. Creating a high-temperature superconductor requires doping a charge transfer insulator. The resulting system has poorly screened dopant ions and structural inhomogeneities. Thus the CDW develops in a system-dependent inhomogeneous electronic environment (22).
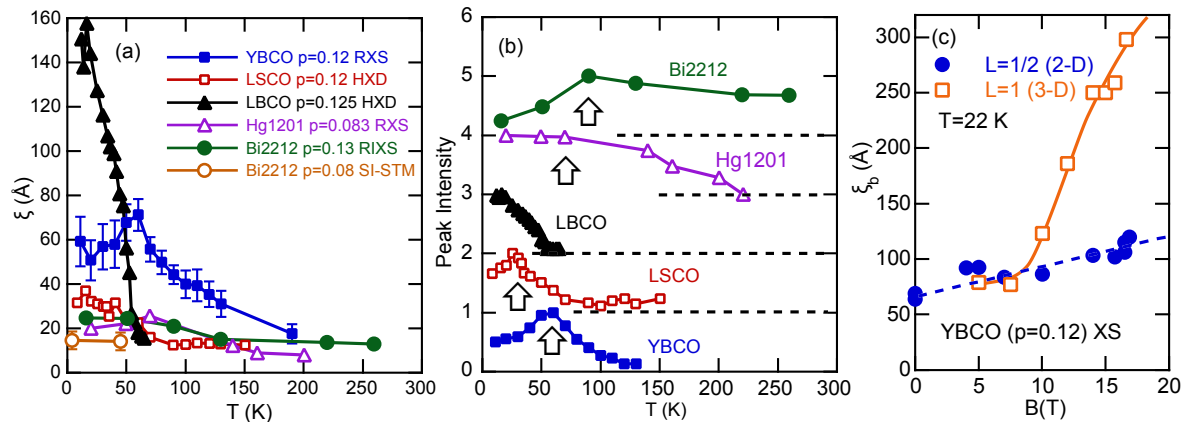
Figure 2

Correlation lengths in cuprates. (a) T-dependence of correlation length ξ for various cuprates (23, 24, 25, 26, 27, 28), ξ is determined from the half-width-at-half maximum peak width (Δ_{HWHM}) in scattering experiments ($\xi = 1/\Delta_{\mathrm{HWHM}}$). (b) T-dependence of CDW Bragg peak intensity. Arrows denote T_c. (c) In-plane correlation lengths vs magnetic field B. For the 2D and 3D components of the CDW (29).

2.1. Correlation Lengths

X-ray scattering scans such as those shown in **Figure 1b-c** can be used to determine the thermal evolution of the CDW correlation lengths, ξ (**Figure 2a**) and CDW Bragg peak intensity (**Figure 2b**) in a range of cuprate families for $p \approx 0.12$. The signal measured is an integral over frequency (energy). For the cuprates, we see that CDW correlations are common and have different and distinct behavior. In the case of LBCO, where the largest ξ is established, ξ grows continuously with the superlattice intensity, distinct from a conventional ordered state. At a different extreme, CDW intensity in Bi2212 and HgBa$_2$CuO$_{4+y}$ (Hg1201) appears at rather high temperatures, but ξ does not grow much and is just comparable to a single CDW period. We define T_{CDW} as the temperature where ξ begins to grow rapidly. For YBCO, the intensity and ξ start to grow at $T_{\mathrm{CDW}} \approx 150$ K, reach a peak at T_c, decrease below that. LSCO shows a rise in intensity and ξ below $T_{\mathrm{CDW}} \approx 70$ K.

Figure 2c provides a teaser to an intriguing behavior found in YBCO that will be discussed further below. At $T < T_c$ and in a magnetic field B applied along the c axis, a new CDW component appears with a much larger ξ. The field (which depresses the superconducting order) also enhances ξ for the low-field CDW component.

2.2. Static Versus Dynamic

CDW correlations involve both static and dynamic components. When discussing CDW order, one usually has in mind static order. Distinguishing between static and dynamic correlations can be challenging. As we will discuss in Sec. 6, there are soft phonons ($E \lesssim 70$ meV) and electronic excitations to which RXS and RIXS are highly sensitive, but where resolving fluctuations from elastic (static) scattering is an experimental challenge.

X-ray photon correlation spectroscopic measurements on CDW scattering from LBCO ($p = 0.125$) at the Cu L_3 edge indicate static speckle patterns over a measurement time of

> 2 h at temperatures up to 45 K (30), providing compelling evidence for "static" CDW order. In YBCO ($p \approx 0.12$), inelastic x-ray scattering (IXS) measurements (31, 32) find that the 2D CDW signal appears static on an energy scale $\hbar\omega \lesssim 1$ meV. ^{17}O NMR measurements on samples with the same doping find similar onset temperatures, providing firm evidence for static order (11).

A Cu L_3-edge RIXS study on YBCO (33), in which energy integration was performed up to 150 meV, found that the CDW scattering could be decomposed into two peaks. The intensity of the narrow peak decreases with temperature in a fashion similar to the previously-identified CDW order, while the broad peak (short ξ) is essentially temperature independent and broad, consistent with dynamic correlations.
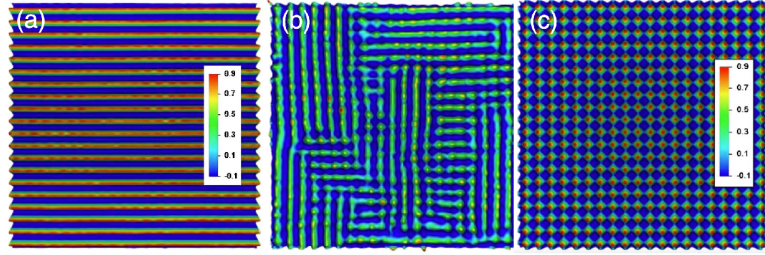
2.3. 1-q and 2-q Order

Figure 3

Real space patterns of charge density. (a-c) Real space patterns of charge correlations from Landau-Ginzburg model with disorder (34). (a) 1-**q** pattern or "stripes". (b) 2-**q** pattern with short range correlations or disorder (a 1-**q** pattern with disorder is indistinguishable (34)). (c) 2-**q** "checkerboard" pattern with long range correlations. Adapted from Ref. (34) with permission.

As a reference point, we now consider the nature of possible broken symmetries introduced by CDW order in a square lattice. The charge density on the lattice sites can be described in terms of two complex scalar order parameters $\varphi_{1,2}(\mathbf{r})$,

$$\rho(\mathbf{r}) = \overline{\rho} + \left[\varphi_1(\mathbf{r})e^{\mathbf{q}_a \cdot \mathbf{r}} + \varphi_2(\mathbf{r})e^{\mathbf{q}_b \cdot \mathbf{r}} + c.c.\right], \qquad 1.$$

where $\mathbf{q}_a \equiv (\delta_a, 0)$ and $\mathbf{q}_b \equiv (0, \delta_b)$. One can write down a Landau-Ginzburg model consistent with the symmetry in terms of these order parameters (34). The interaction between them is controlled by the coupling term $\gamma|\varphi_1|^2|\varphi_2|^2$. If $\gamma > 0$, then φ_1 and φ_2 effectively repel each other, so that a 1-**q** "stripe-like" structure (**Figure 3a**) is favored. On the other hand, if $\gamma < 0$, there is effective attraction and a 2-**q** "checkerboard-like" pattern (**Figure 3c**) is favored. When ξ is long, there is a clear distinction between 1-**q** and 2-**q** order. However, in real materials with a short correlation length, the distinction is not clear, as one can see from the simulation of disorder effects in **Figure 3c** (34).

Diffraction from a cuprate with a square lattice (35) and NMR in general (21) cannot be unambiguously inverted to produce the real space variation of the order parameter. Given that it provides real-space images, SI-STM is the ideal way to see whether there is a preference between 1-**q** and 2-**q** pictures. The challenge is that imaging over a large area requires materials that cleave well, and these systems, even when orthorhombic, tend to have equivalent Cu-O bonds in orthogonal directions and short correlation lengths (36, 37).

In systems where there is broken rotational symmetry between Cu-O bonds , or symmetry is broken by uniaxial stress (see Sec. 4), clear distinctions are possible.

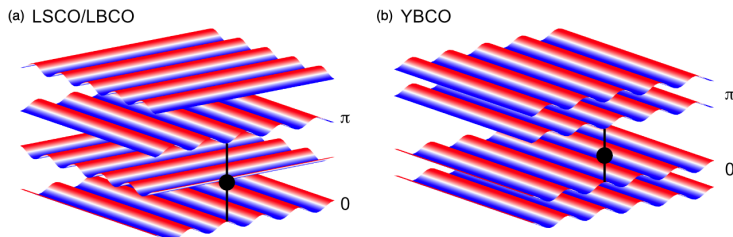## 2.4. 2D and 3D Orders

(a) LSCO/LBCO   (b) YBCO

Figure 4

The schematics show how inter-plane correlations might develop due to interaction with a dopant site or Coulomb interactions in (a) LSCO/LBCO and (b) YBCO. The phase of the CDW order parameter is denoted by the color and the black sphere represents an out-of-plane defect.

The CuO_2 layers in which CDW correlations develop are stacked in 3D structures along the crystalline c axis. What about correlations along the c axis? For CDW scattering characterized by $\mathbf{q}_a$, the 3D wave vector is $\mathbf{Q} = (\delta, 0, \ell)$. If there were no correlations between neighboring planes, the scattering at $\mathbf{Q}$ would be independent of ℓ. If the CDW order were exactly the same and in phase in all layers, then the scattering would peak at $\ell = n$, where n is an integer (which appears to be the case in Hg1201 (26)). It turns out that measurements of CDW scattering in Nd-LSCO (38), LBCO (39), YBCO (13), and LSCO (24) find that the intensity has a broad peak at $\ell = n + 1/2$. Such a peaking in ℓ indicates that the CDW correlations exhibit a doubling along c with respect to the crystallographic unit cell. The significance depends on the crystal structure and the nature of the correlations. A broad peak in ℓ (13, 24) indicates a limited correlation length along the c-axis.

For LBCO and similar compounds, the CDW order occurs in a structure that has broken rotational symmetry of the Cu-O bonds, with an orientation that rotates $\pi/2$ between neighboring layers (see Sec. 4), correspondingly, the 1-$\mathbf{q}$ order rotates its orientation, as shown in **Figure 4a**. Coulomb repulsion between the charge modulations in the layers favors a π phase shift of the CDW order in the next-nearest neighbor layers, as indicated. A recent x-ray study indicates how this is communicated between layers by displacements of the out-of-plane ions (40), resulting in a "3D" CDW order. The random distribution of dopant ions presumably limits the correlation length along c.

In YBCO, the π phase shift illustrated in **Figure 4b** appears to arise from quenched disorder in the chain layer (41, 42) resulting in anomalies in the Coulomb potential. The response is the same CDW configuration within the neighboring CuO_2 bilayers, but with out-of-plane displacements occurring in opposite directions. It is convenient to label this order with short c-axis correlation length, observed in low magnetic fields, as a "2D" CDW to distinguish it from the 3D CDW order that can be induced by the application of a c-axis magnetic field ($\gtrsim H_{c2}$) (43, 29), uniaxial stress (44) or strain due to a substrate (45). This

3D component is also a 1-$\mathbf{q}$ CDW, peaked at wavevectors such as $(0, \delta_b, 1)$. It has relatively long correlation lengths of $\xi_b \approx 300$ Å (see **Figure 2c**) and $\xi_c \approx 50$ Å (29).

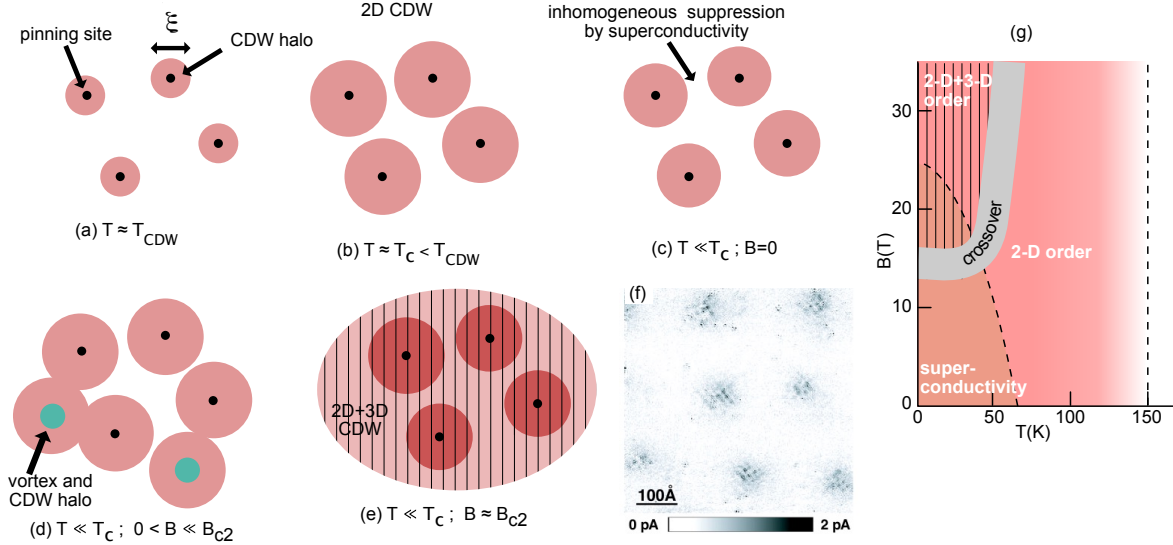## 2.5. Pinning, Nucleation, and the Effect of a Magnetic Field

Figure 5

Schematic representation CDW order in cuprates. Pink regions of typical size ξ are where a defect nucleates the CDW or disrupts the phase of the CDW order parameter. (a) CDW halos or puddles nucleate on pinning sites. (b) Correlation length increases as T reduced to T_c. (c) CDW is suppressed inhomogeneously in the superconducting state ($B = 0$). (d) Superconducting state in small fields. Vortices are introduced and additional CDW correlations appear as "vortex halos". (e) At high fields, 2-D CDW is strengthened and a second 3-D 1-$\mathbf{q}$ component appears, this locks in to form 3-D CDW order (43, 29, 46) (f) SI-STM image of local density of states in showing density correlations associated with vortices $Bi_2Sr_2CaCu_2O_8$. The image shows the difference of data collected in the superconducting state, with and without a magnetic field of 5 Tesla illustrating the vortex halos. Image from Ref. (16) with permission. (g) $B-T$ phase diagram based on (11, 43, 29, 46).

In conventional CDW systems, the properties of the CDW are intimately connected to quenched disorder and the periodic ("lock-in") potential of the host lattice (47, 48). McMillan (47) showed that pinning sites (due to dopants and impurities) lead to a local enhancement of the ordered phase and stabilize the incommensurate phase relative to the commensurate.

Figure 5a-c presents a schematic representation of the development of 2-D CDW order in a cuprate such as YBCO on cooling. In the doping regime ($p \sim 0.12$) where CDW correlations are maximized, **Figure 5a** indicates the situation near the onset of CDW order, where, in analogy with the STM results of **Figure 5e** (16), it is reasonable to expect that the CDW modulations (with 2-$\mathbf{q}$ CDW character) appear in halos or puddles centered on the defects (49). For YBCO, because the crystal structure is orthorhombic, it is possible for x-ray diffraction on detwinned crystals to detect CDW peaks characterized

by both $\mathbf{q}_a$ and $\mathbf{q}_b$ (50, 23). The halos and correlation length grow on cooling towards T_c (**Figure 5b**). The disorder disrupts inter-halo coherence (49) leading to a finite ξ. The scattered intensity and ξ decrease below T_c (**Figure 2**) due to inhomogeneous competition with the superconducting state (**Figure 5c**).
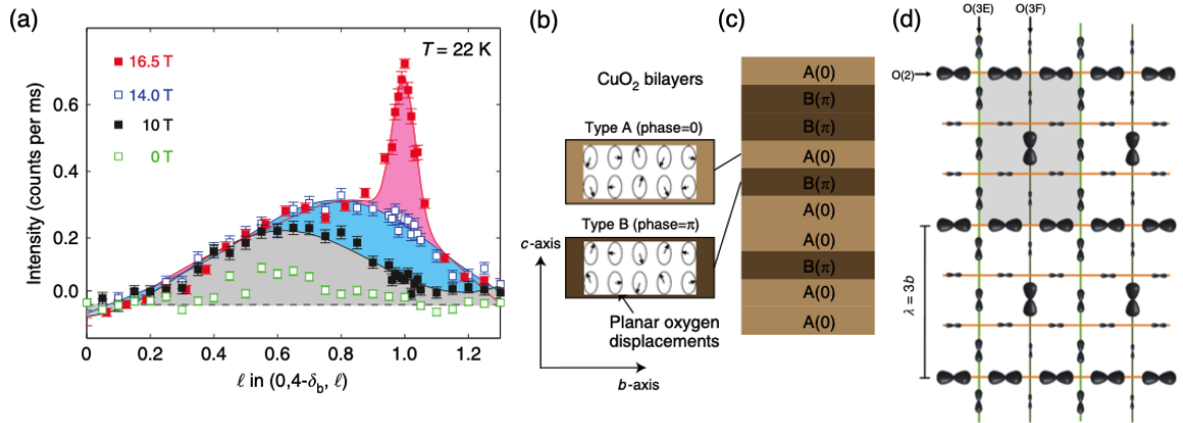
The effect of magnetic field on CDW in YBCO. (a) Intensity of the CDW Bragg peak vs ℓ (c-axis wavevector) showing how inter-planar correlations develop. 2-D correlations (centered on $\ell \approx 1/2$) are enhanced with field and 3-D ($\ell = 1$) CDW order develops above $B \approx 10$ T (29). (b-c) 3-D CDW order develops as the single bilayer CDW structure (with broken mirror-plane symmetry) becomes coherent along the c-axis (29). (d) For $B \gtrsim 10$ T a locked-in structure with period $3b$ develops in local regions separated by discommensurations (46). Panels (a-c) adapted from Ref. (29) (CC BY 4.0), (d) reproduced from Ref. (46) (CC BY 4.0).

As we have noted, application of a c-axis magnetic field to the superconducting phase introduces quantized superconducting vortices within the CuO_2 planes. Given that the superconducting order goes to zero in the vortex core and that it only gradually recovers strength with distance from the core, it is quite plausible that a competing phase of CDW order will develop in a halo region about the core, as illustrated by the STM image measured on Bi2212 (16) in **Figure 5f**. Hence, as indicated in **Figure 5d**, we expect that applying a modest magnetic field to YBCO in the superconducting phase will induce vortices with CDW halos in regions away from defect-pinned CDW puddles. On approaching the critical field B_{c2}, the superconducting order will be gradually suppressed, as there is overlap of the CDW halos, and longer-range order (11) develops. Without the CDW order, B_{c2} would correspond to the point at which vortex cores fill the plane. Since the CDW halos are much larger, B_{c2} is correspondingly decreased (51, 52).

NMR (46) and x-ray diffraction (43, 29) measurements provide direct support for this picture. The competition between CDW pinning and the stiffness of the CDW order parameter leads to a "crossover (broadened) transition" to a state with long range 3D order (21, 11, 43, 29, 49, 42, 46) which coexists locally (11) with the 2D order. The evolution of the CDW correlations is most dramatically seen in the diffraction measurements of the ℓ-dependence of the intensity of $\mathbf{q}_b$ correlations, $I(0, \delta_b, \ell)$ (43, 29) as shown in **Figure 6a**. For $B = 0$, $I(0, \delta_b, \ell)$ shows a weak and broad peak at $\ell \approx 1/2$ corresponding to the 2D correlations discussed in Sec. 2.4. For $B = 10$ T, the 2D CDW correlations are enhanced as superconductivity is suppressed, and at $B = 16.5$ T a new Bragg peak appears at $\ell = 1$

corresponding to the 3D order.

Besides the field-induced enhancement of the intensity associated with the 2D CDW correlations, there is also a shift in the position in ℓ of the intensity maximum (**Figure 6a**). The low-field scattering pattern is a consequence of the broken mirror-plane symmetry of the CuO_2 bilayers (see Sec. 2.7). The CDW structure can be represented by a sequence of layers with Type A (phase=0) and Type B (phase=π) modulations as shown in **Figure 6b**. The evolution of the ℓ-dependent scattering with field can be modeled by changing the balance of the A and B modulations along the c axis, as suggested in **Figure 6c** (29).

The 3D CDW order that appears above ~ 15 T is a unidirectional (1-**q**) modulation along the b axis with enhanced correlation lengths both in-plane (**Figure 2c**) and along the c axis (43, 29, 53). Recent NMR measurements (46) indicate that the CDW locks in locally with $\delta_b = 1/3$ for $YBa_2Cu_3O_{6.56}$ ($p = 0.109$) (**Figure 6e**). This is interesting because the wave vector measured in high-field x-ray experiments on the 3D CDW (54) find $\delta_b = 0.314(2)$ for $YBa_2Cu_3O_{6.67}$ ($p = 0.123$). The difference can be accounted for by the CDW having regions where the local structure has period $\lambda = 3a$ with phase slips (discommensurations) between these regions (46). Similar behavior is seen in other CDW systems such as $TaSe_2$ (55) and also in STM measurements on Bi2212 (56).

The B-T phase diagram for the 2D and 3D CDW orders is shown in **Figure 5g**. Interestingly, the 3D order only appears at low temperature, in a range comparable to the superconducting phase that it replaces, while the shorter-range 2D correlations extend to higher temperatures.

The impact of pinning and structure varies among cuprates. In the case of LBCO, the dopants are relatively dense. They determine the landscape within which the CDW order occurs (57), but ξ is large relative to the average defect spacing.

2.6. Competition with superconductivity

In general, CDW correlations tend to show optimal strength at a hole concentration $p \sim 0.12$, with a corresponding depression of T_c (relative to a dome that varies parabolically with p) (1). For YBCO, plotting the upper critical field H_{c2} versus p yields peaks at $p_1 \approx 0.08$ and $p_2 \approx 0.08$, and a minimum near $p \approx 1/8$ (52). Also for YBCO, in zero magnetic field the CDW peak signal grows on cooling toward T_c, and then decreases below T_c (but not to zero) and ξ also decreases below T_c (12, 13). These observations suggest competition between superconductivity and the CDW.

When $T_c(B = 30$ T) is plotted versus p for YBCO we see suppression around $p \sim 0.12$, with a weak peak at $p_1 \approx 0.08$ and a large peak at $p_2 \approx 0.18$ (52). Thus YBCO has a lot in common with LBCO in zero field. LBCO shows a sharp dip in T_c for bulk superconductivity at $p = 1/8$, which corresponds with optimal CDW order (58, 59). Both the CDW order in LBCO and the 3D CDW order in YBCO appear to be 1-**q** states. It must be noted that, while the bulk superconducting order is strongly depressed in LBCO $x = 1/8$, mean-field 2D superconductivity onsets at 40 K (60), together with SDW order. The presence of 2D superconductivity without 3D order has been rationalized in terms of pair-density-wave (PDW) order (61). The best evidence for PDW order comes from a recent SI-STM study of the vortex-halo CDW order in Bi2212 (62, 61).

Applying a c-axis B field to LBCO $x = 1/8$ has little impact on the CDW order, as there is little bulk superconductivity to suppress. The situation is different for LSCO with $p \approx 0.12$, where x-ray diffraction finds that the CDW intensity present at zero field doubles
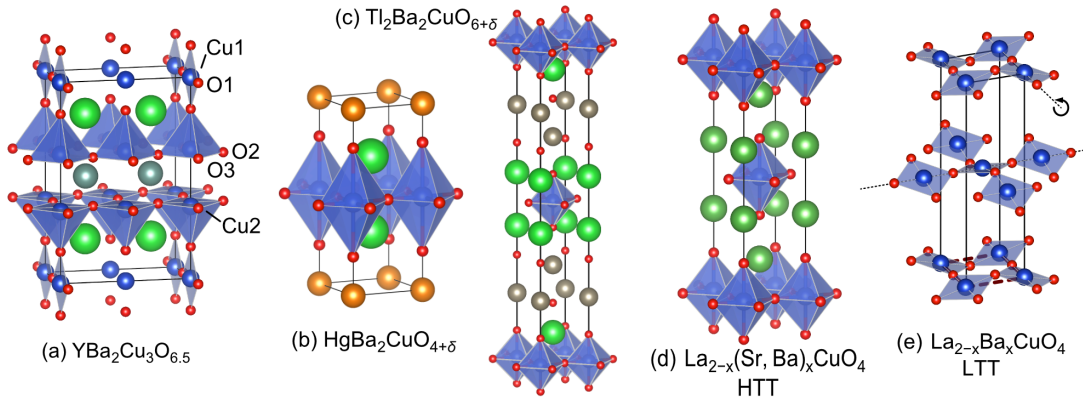
Figure 7

Crystal structures of selected cuprates. (a) $YBa_2Cu_3O_{6.5}$ is the ortho-II (chain ordered) structure. For LBCO LTT (e), the shaded squares are center sections of CuO_6 octahedra shown the HTT structure. The octahedral rotations about the Cu−O bonds are exaggerated by a factor of 5. The dashed lines illustrate the bond buckling in the direction perpendicular to the rotation axis, which may favor 1-$\mathbf{q}$ charge and spin order. Figure produced with VESTA (65).

with a c-axis field of 10 T (63, 64).

2.7. Displacement Patterns

The displacement pattern of the cuprate CDWs may be determined (66, 40) by measuring a reasonable number of satellite Bragg peaks by x-ray or neutron diffraction and fitting measured intensities to ones calculated from possible models. The concept of a continuous phase transition, as described by Landau theory, involves the loss of a symmetry of the parent structure. The orthorhombic phase of YBCO has relatively high-symmetry ($Pmmm$), which means that there are relatively few displacement patterns, or irreducible representations (IRs), that are consistent with the ordering wave vectors (66, 68). An analysis based on the observed superlattice peaks indicates that the mirror-plane symmetry of the Cu-O chain layer (**Figure 7a**) is retained but that of the CuO_2 bilayers is broken.

The CDW structure consistent with the x-ray scattering data for $YBa_2Cu_3O_{6.54}$ (Ortho-II, $T_c \approx 60$ K) (66) can be described as a sum of displacements associated with modulations $\mathbf{q}_a$ and $\mathbf{q}_b$. For the parent structure, let the atomic positions, lattice points and unit cell atomic positions be denoted $\{\mathbf{r}_{ld}\}$, $\{\mathbf{r}_l\}$ and $\{\mathbf{r}_d\}$, with $\mathbf{r}_{ld} = \mathbf{r}_l + \mathbf{r}_d$. For the $\mathbf{q}_a$ modulation, the atomic displacements due to the CDW are given by a sum of two terms, one polarized along $\mathbf{c}$ ($\mathbf{u}_d^c$) and the other polarized along $\mathbf{a}$ ($\mathbf{u}_d^a$). The displaced atomic positions are

$$\mathbf{r}'_{ld} = \mathbf{r}_{ld} + \mathbf{u}_d^c \cos(\mathbf{q}_a \cdot \mathbf{r}_{ld} + \varphi) + \mathbf{u}_d^a \sin(\mathbf{q}_a \cdot \mathbf{r}_{ld} + \varphi), \qquad 2.$$

where symmetry requires that the $\mathbf{u}_d^c$ and $\mathbf{u}_d^a$ displacements are $\pi/2$ out of phase and there is an analogous expression for the displacements associated with $\mathbf{q}_b$.

The intriguing CDW structure determined from x-rays is summarized in **Figure 8a-d**. The overall structure of the $\mathbf{q}_b$ mode is shown in **a**, where it can be seen that the ionic displacements are largest within the CuO_2 planes. The in-plane oxygen atoms have the largest displacement amplitudes, $\approx 4 - 5 \times 10^{-3}$ Å. The displacements for the $\mathbf{q}_a$ mode (not shown) are similar. The displacement pattern is made up of a superposition of the
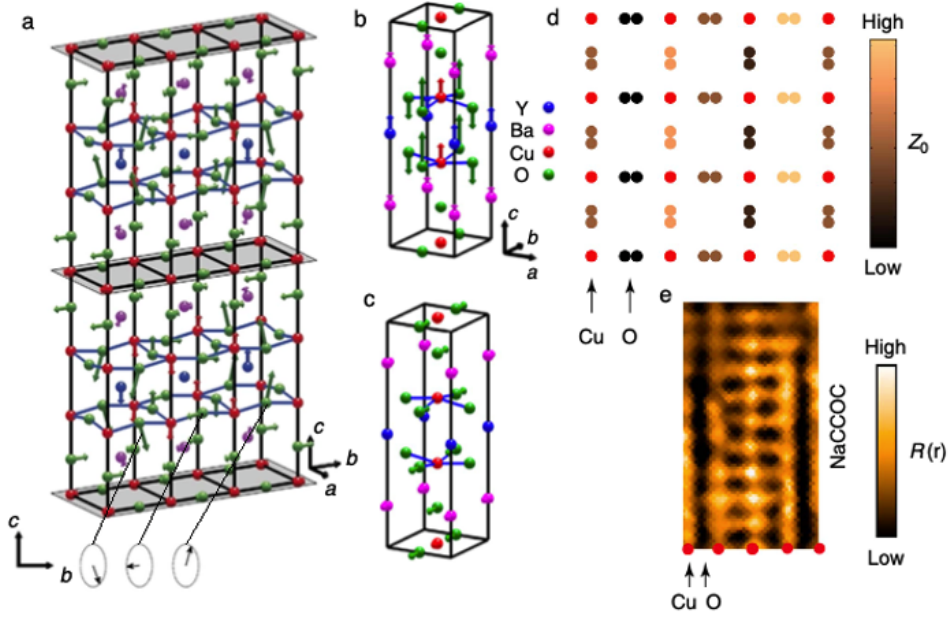
Figure 8

Displacement pattern of CDW in YBCO determined from x-ray diffraction (66). (a) Arrows represent the atomic displacements. Oxygen atoms show the largest displacements. Remaining mirror planes in CDW structure show in grey. The modulation is constructed from the motifs in (b) and (c) which are $\pi/2$ out of phase. (d) From STM measurements on $Ca_{2-x}Na_xCuO_2Cl_2$ (NaCCOC) (67), the ratio of the tunneling current measured at a bias voltage of $+150$ meV relative to -150 meV shows the d-wave form factor. Panels (a-d) reproduced from Ref. (66) (CC BY 4.0), panel (e) reproduced with permission from Ref. (67).

motifs in **Figure 8b** and **c** modulated in space according to Equation 2. This means that the direction of the displacement of a given atom in the unit cell precesses as we move along the b-axis as shown in **Figure 8a**. The displacement pattern of the in-plane oxygen atoms along the c-axis is plotted for the a-b plane in **Figure 8d**. This pattern may be viewed as a d-wave form factor (67) associated with the Cu sites in that the displacements along perpendicular Cu-O bond directions are out of phase. A similar pattern is seen in STM measurements on another cuprate (67), as shown in **Figure 8e**, suggesting that the displacement pattern is associated with a modulation of the local electronic structure. The d-wave form factor is also seen in RXS measurements (69). However, an s-like symmetry was identified by RXS for LBCO $p = 1/8$ (70), and a recent study indicates an s component in YBCO (71).

3. Spin Density Waves and Spin Fluctuations

Cuprate superconductors show spin fluctuations that are strongest near $\mathbf{q} = (1/2, 1/2)$ and have energies up to ~ 300 meV. Thus, charge order forms in a background of strong antiferromagnetic correlations. Some cuprates, including Nd-LSCO (72, 73), Eu-LSCO (74), LBCO (58, 75) and LSCO also show freezing or ordering into a spin density wave (SDW) for

$T \lesssim T_{\mathrm{CDW}}$ in which the wave vectors of the SDW and CDW are related. Diffraction peaks due to the SDW occur at $(1/2, 1/2 \pm \delta_s)$ and $(1/2 \pm \delta_s, 1/2)$ with $\delta_c = 2\delta_s$. This relationship of δ_c and δ_s occurs naturally in the stripe picture mentioned in Sec. 1.2. Note that the cuprates with strong SDW order also have a strong suppression of bulk superconductivity, as discussed in Sec. 2.6.

It is natural to ask how universal the δ_c and δ_s are among cuprates. We plot the doping dependence of these for a number of cuprates in **Figure 9**. For δ_s, we compare the SDW results for LBCO with results for the lowest-energy incommensurate excitations in YBCO and Bi2201, and find a similar trend. In contrast, there are distinct behaviors for δ_c vs. p. The relation $\delta_c = 2\delta_s$ holds only in those systems, mentioned above, that exhibit SDW order. In contrast, systems with suppressed low-energy spin fluctuations, such as YBCO (50, 76, 23, 77, 78) and Bi2201 (79, 80), show no obvious relationship between δ_s and δ_c.
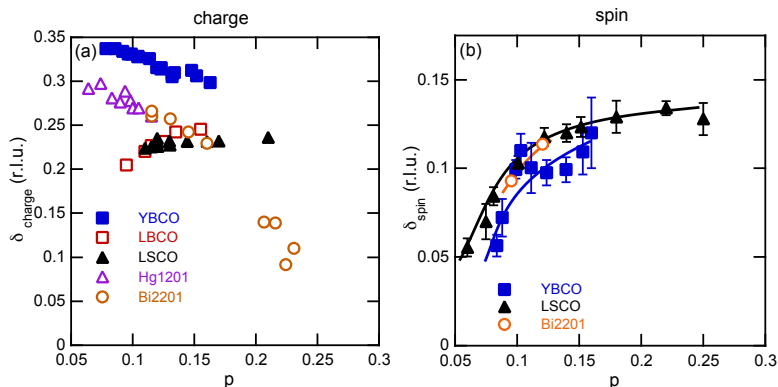

Figure 9

Comparison of propagation vectors (δ_c and δ_s respectively) associated with CDW and low-energy spin fluctuations as a function of doping for selected materials. (a) For CDW case, wavevector is $(0, \delta_c)$. Data from Refs. (50, 76, 23, 59, 24, 81, 82, 26, 83, 79). (b) For spin case wavevectors are $(1/2, 1/2 \pm \delta_s)$ and $(1/2 \pm \delta_s, 1/2)$. Data from Refs. (77, 78, 84, 80)

4. Relationship between the CDW and crystal structure

The common structural feature of the cuprate superconductors is the CuO_2 plane. Thus, it is the electronic properties of the these planes that almost certainly drive the formation of the CDW, and provide the primary order parameter. The CuO_2 planes can be embedded in a variety of host structures with different crystal symmetries, and a few examples are illustrated in **Figure 7**. A very clear case of coupling of the CDW to the crystal structure occurs for the $La_{2-y}(Nd)_y(Sr,Ba)_xCuO_4$ system. Members of this system such as Nd-LSCO (x=0.12) (14) and LBCO ($x = 0.125$) (59) exhibit a phase transition to the low-temperature-tetragonal (LTT) structure (see **Figure 7**) at T_{LTT}. It is found that $T_{\mathrm{CDW}} \lesssim T_{\mathrm{LTT}}$ in both cases. The distortion of the CuO_2 planes in the LTT phase, as shown in **Figure 7e** involves different Cu-O bond lengths in orthogonal directions, which provides a unique orientation

for a 1-**q** CDW order in each plane, with a $\pi/2$ rotation between planes.

The situation in the sister compound LSCO is more subtle. For LSCO ($x \approx 1/8$), there is a transition from the HTT structure of **Figure 7d** to the low-temperature-orthorhombic (LTO) structure below $T_{\mathrm{LTO}} \approx 240$ K in which the CuO_6 octahedra rotate about the [110]-type directions. Recent studies have found evidence for extra distortions of the nominal LTO phase (85, 86) resulting in inequivalent Cu-O bonds in (approximately) orthogonal directions (though with a smaller difference than in the LTT phase). This enables an onset of CDW order at $T_{\mathrm{CDW}} \approx 70$ K (24, 87), which is higher than the T_{LTT} of LBCO. Applying a uniaxial compressive stress along one of the Cu-O bond directions has recently been used to prepare a CDW with macroscopic 1-**q** character. CDW and SDW orders are suppressed in the direction of compression and substantially enhanced in the orthogonal direction (64, 88). It seems likely that this is due to the single domain 1-**q** CDW being favored by further structural distortions induced by the uniaxial stress (85).

In YBCO, the 4-fold symmetry of the CuO_2 planes is broken by the Cu-O chain order **Figure 7a**. The resulting orthorhombic structure has distinct Cu-O bond lengths along the a and b axes, with $a/b \approx 0.99$ (50). The 2-D 2-**q** charge correlations, most likely nucleated by defects, develop under this orthorhombic perturbation as discussed in Sec. 2.5. In contrast, the 3-D 1-**q** order that is induced in high magnetic field chooses a unique 1-**q** orientation, with its modulation along the b axis (parallel to the Cu-O chains) (43, 29). Intriguingly, application of uniaxial stress perpendicular to the chains in YBCO with $p = 0.12$ induces the same 1-**q** 3D order at $T_{\mathrm{CDW}}^{\mathrm{3-D}} \approx 70$ K, before disappearing at lower temperature as bulk superconducting order appears (44). In Hg1201 and Bi2212, the CDW correlation length remains short at low temperature (**Figure 2**) blurring the distinction between **1-q** and **2-q** order (89, 90).

5. Fermi surface reconstruction: Hall coefficient and Quantum oscillations

The formation of charge- or spin-density wave order can lead to Fermi surface (FS) reconstruction and, in some cases, to dramatic changes in transport coefficients. For example, in $NbSe_2$ the T-dependence of the Hall coefficient (R_H) and the thermopower (S) deviate from their high-T trends at $T_{\mathrm{CDW}} \approx 32$ K (93). Similar behavior is observed in YBCO ($p = 0.12$) (91) as shown in Fig. 10(a) where we see that $R_H(T)$ begins to show a downturn from its high-T trend near T_{CDW} and changes sign at low T. Thus, charge order is an obvious candidate to explain reconstruction of the Fermi surface (20, 92) resulting in the formation of closed electron-like pockets (**Figure 10b**) detected by quantum oscillations (QO) (18). The onset of the 2D CDW, with its 2-**q** character, naturally explains (20) the sign reversal observed (91) in the Hall number $n_H = 1/R_H$ at low-temperature for doping $p < 0.16$. In the overdoped cuprate $Tl_2Ba_2CuO_{6+\delta}$ (Tl2201), a $p \rightarrow 1 + p$ transition is observed in the high-field limit of n_H, where the $1 + p$ behavior is found for $p > 0.25$ (94), consistent with QO measurements that indicate a large pocket in that range (95). The crossover has been shown to correlate with the disappearance of the CDW in this compound (83).

The 2-**q** nature of the 2D CDW in YBCO ($p \approx 0.12$) provides a plausible way to explain the QO measurements (96, 19, 20, 97). However, one issue may be the limited correlation length ξ_{2D}, which is $\xi_{\mathrm{2D}} \approx 100$ Å at $B = 15$ T and could increase further with field (**Figure 2c**). The relevant length scales for comparison are the radius of the QO orbit in real space, which can be estimated from the QO frequency as $r_{\mathrm{orbit}} = \sqrt{2\hbar F/(eB^2)} \approx 150$ Å (18), and the quasiparticle mean free path $l_0 = v_F\tau \approx 200$ Å (98) for YBCO ($B = 55$ T).
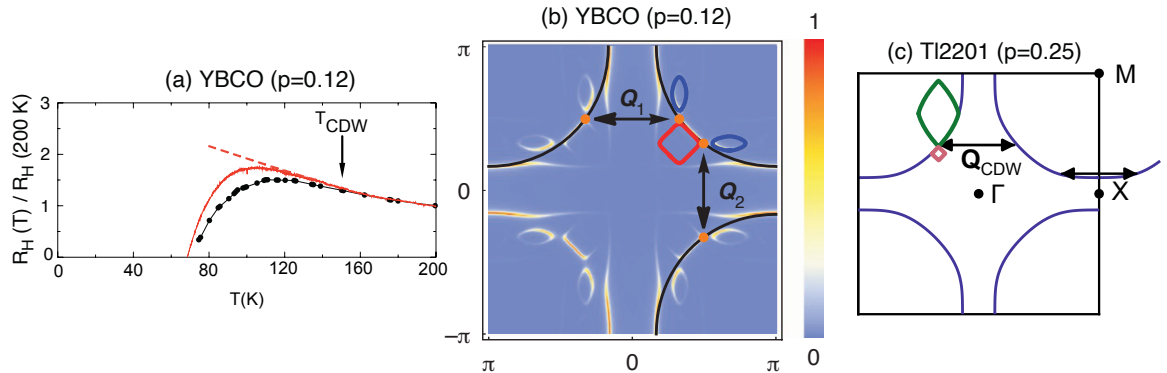
Figure 10

Fermi surface reconstruction in cuprates. (a) In YBCO, on cooling, the Hall coefficient shows a deviation from its trend line beginning near T_{CDW}. There is a downturn and eventual sign charge (91). Adapted from Ref. (91) with permission. (b) CDW order combined with the momentum-dependent pseudogap cause FS reconstruction in YBCO (20, 92). The electron pocket (red) is believed to be responsible for the quantum oscillations seen in this system (18). Adapted from Ref. (92) (CC BY 4.0). (c) The CDW observed in Tl2201 should also produce FS reconstruction, in this case the hole pocket (green) is larger than the electron pocket (red) (83).

While the 3D CDW has a longer correlation length, its 1-**q** character makes an explanation of the small pocket more challenging (97). For the 2D CDW, ξ_{2D} is roughly comparable to r_{orbit} and ℓ_0. It is also relevant to note that a recent experiment measuring the Hall effect in the presence of uniaxial stress found no change in behavior in the temperature range where the 3D CDW is induced (99). Hence, the 2-**q** picture remains the popular explanation for the FS reconstruction and QO results. Multiple QO frequencies observed in YBCO (100) are thought to be due to the CDW breaking the mirror plane symmetry of the bilayer (101, 102). QO have also been observed in Hg1201 (103, 104), however, in Hg1201 (26) the CDW has a much shorter correlation length, $\xi \approx 20{-}30$ Å, than in YBCO.

6. Charge Excitations and Phonon Anomalies

So far in this review we have concentrated on the charge correlations with wave vectors $\mathbf{q} \approx (\delta, 0)$, with $\delta = 0.2{-}0.3$, that are at least quasi-static on the scale of $\hbar\omega \sim 1$ meV. Collective charge excitations can be observed directly using probes such as electron energy loss spectroscopy (EELS) (110) and RIXS (111, 105), or via their coupling to phonons using inelastic x-ray scattering (IXS), neutron scattering (INS) and RIXS.

Recent advances in RIXS have allowed the observation of dispersive collective charge excitations in cuprates with energies up to ~ 1 eV (111, 105). **Figure 1a** shows a schematic representation of where these lie in **q**-space. In a conventional picture of a metal (which does not apply directly to cuprates), we expect the charge response $\chi_c(\mathbf{q}, \omega)$ to be approximated by a random phase approximation (RPA) or similar theory to include Coulomb interactions together with a Lindhard function (112). This will lead to plasmons and damped but structured 'electron-hole' excitations. In 3D metals, the plasmon has a large gap $\omega_p \approx ne^2/(2m^\star\epsilon)$. However, the cuprates behave approximately as 2D conducting sheets separated by dielectric blocks. This geometry leads to "acoustic plasmons" (112)
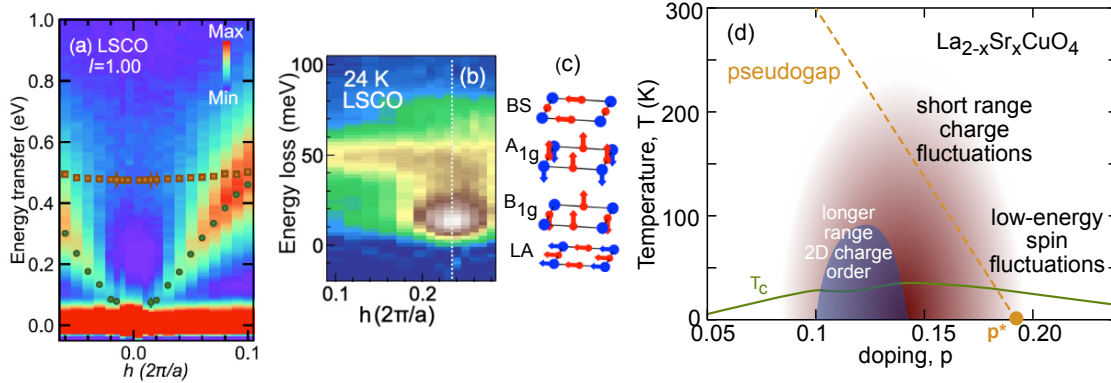
Figure 11

Collective charge excitations in cuprates. (a) Acoustic plasmon excitations measured in LSCO($p = 0.16$) using O-K RIXS (105). Figure from Ref. (105) with permission. (b) Signatures of collective charge excitations measured near $\mathbf{q}_{CDW}$ in LSCO($p = 0.15$) measured with O-K RIXS with ∼16 meV resolution. (106). An elastic ($E = 0$) peak has been subtracted from the data. Scattering due to charge excitations and coupling to various phonon modes is seen at $\mathbf{q}_{CDW}$ over the energy range $10 - 70$ meV. Figure from Ref. (106) (CC BY). (c) Oxygen phonon modes in a single CuO$_2$ layer: in-plane bond-stretching mode (BS); the in-phase A_{1g} and out-of-phase B_{1g} c-axis polarized modes; and the longitudinal acoustic (LA) mode (107, 106). (d) Nature of CDW correlations in LSCO with doping and temperature (108, 109).

which have out-of-phase charge oscillations in neighboring layers that disperse to energies ≲100 meV for certain values of the c-axis wave vector. Acoustic plasmons or a strongly-dispersing electron-hole continuum have been observed for $h \lesssim 0.1$ in electron- (111) and hole-doped (105) cuprates using Cu-L_3 and O-K edge RIXS, respectively. **Figure 11a** shows the acoustic plasmons in LSCO ($p = 0.16$) (105).

Evidence for charge density fluctuations near $\mathbf{q}_{CDW}$ was initially provided by their coupling to phonons. A dip in the dispersion of the Cu-O bond stretching mode along the Cu-O bond direction at $\mathbf{q}_{CDW}$ was identified by inelastic neutron scattering studies of YBCO (113) and 214 cuprates (114).

The acoustic phonons in conventional CDW systems such as NbSe$_2$ show a dip in their dispersion near $\mathbf{q}_{CDW}$ which tends to zero frequency as $T \to T_{CDW}$ (**Figure 12c**). In YBCO, a broadening is observed at T_{CDW} where the 2D CDW order develops (**Figure 12a,b**). It is not clear whether there is an associated softening at ambient pressures. However, a complete softening is observed when 3D CDW order is induced under uniaxial pressure (44). In LBCO (115) and Bi2212 (116), phonon anomalies at $\mathbf{q}_{CDW}$ are found to persist for $T > T_{CDW}$. Thus, it appears that the phonon broadening observed in YBCO and the other systems signals the presence of charge correlations or a precursor effect, rather than the 2D CDW order.

Theoretical analysis (107, 106) has demonstrated the sensitivity of RIXS measurements to phonon modes involving the O atoms within the CuO$_2$ planes, especially: the in-plane bond-stretching mode (BS); the in-phase A_{1g} and out-of-phase B_{1g} c-axis polarized modes; and the longitudinal acoustic (LA) mode. RIXS measurements on LSCO ($p = 0.15$) at the O K edge (106), shown in **Figure 11b**, demonstrate this sensitivity. The feature at ∼ 14 meV and the column of scattering at $h = q_{CDW} \approx 0.24$ result from CDW fluctuations
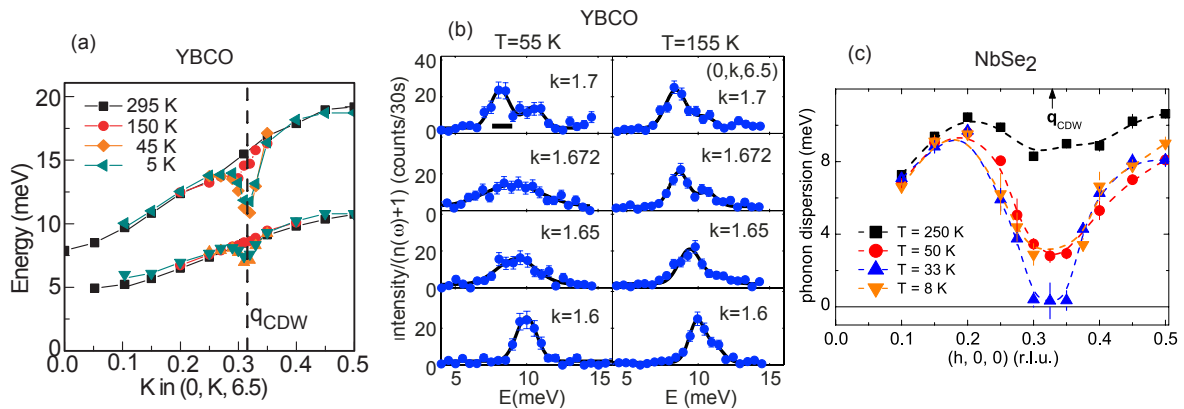
Figure 12

Acoustic phonon anomalies. (a) YBCO (p=0.12) shows T-dependent anomalies in the acoustic phonons near $\mathbf{q}_{\mathrm{CDW}}$. These have been interpreted on terms of a softening (a) (32) or broadening (b) (31) of the excitations. Panel (a) from Ref. (32) with permission. (c) A phonon softening at $\mathbf{q}_{\mathrm{CDW}}$ is seen in NbSe$_2$, with the phonon frequency tending to zero at T_{CDW} (117). Figure from Ref. (117) with permission.

and their coupling to acoustic and other phonons. Related features are seen at the Cu-L_3 edge in YBCO (33, 118) and Bi2212 (27). In both cases the scattering increases in strength and has a decreasing characteristic energy with reducing T.

In this review have have discussed two components to the charge correlations near $\mathbf{q}_{\mathrm{CDW}}$: A quasistatic, longer-range component with $\xi \sim 100$ Å (CDW-order) and shorter-range ($\xi \sim 20$ Å) inelastic (dynamic) component with characteristic energy $\hbar\Gamma \sim 10-100$ meV (charge density fluctuations). A recent study of LSCO and Eu-LSCO (108) has analyzed measurements in terms of these two components and argues that the CDW order is only found below approximately optimal doping, while the charge density fluctuations exist to higher dopings. **Figure 11d** shows how the charge correlations vary with T and p based on this picture (108, 33, 109). There have been various proposals of a quantum critical point (QCP) near $p^\star$. Recent measurements on YBCO suggest that the dynamic-charge density fluctuations soften as p approaches $p^\star$ (33, 118). However, the CDW order tends to disappear at lower doping in this system.

7. Theoretical perspectives on CDW order in cuprates

Early studies of the hole-doped antiferromagnet problem found Hartree-Fock solutions that corresponded to CDW and SDW order, but with an insulating nature (due to the ratio of doped-hole density to the CDW period) (119, 120, 121). Alternatively, an effective model for competition between short- and long-range interactions (frustrated phase separation) also found evidence for stripe and checkerboard phases (122), checkerboard charge order was also evaluated in Ref. (123). A different take ignores the spin correlations and attributes the non-Fermi-liquid behavior to scattering from CDW fluctuations (124), especially in association with a proposed CDW quantum critical point (125).

A new approach of numerical computations to solve the 2D Hubbard model (and re-

lated simplifications such as the t-J model) began with the application of the Density Matrix Renormalization Group (DMRG) by White and Scalapino (126). New numerical variations have been introduced, providing evidence that combined CDW and SDW states (with pairing correlations) are close in energy to a state with uniform d-wave superconductivity (127). Dynamic CDW and SDW correlations are seen in quantum Monte Carlo (QMC) calculations, where calculations are only possible at a relatively high temperature (128). The numerical techniques mentioned so far are all in real space, but a recent study has found consistent results for intertwined CDW and SDW correlations obtained with one QMC technique solved in reciprocal space and another in real space (129). This is an active and evolving field; for a broad review of work on the Hubbard model see Ref. (130).

8. Summary and Perspectives

This review, together with many studies of spin excitations (131), demonstrates how spin and charge fluctuations pervade the phase diagram of the cuprates. Theory suggests that spin fluctuations near $\mathbf{q} \sim (1/2, 1/2)$ are responsible for the pseudogap behavior which collapses around $p^\star \sim 0.19$ (see Ref. (132) for recent references). Collective charge fluctuations with $Q = (\delta_c, 0)$ ($\delta_c \approx 0.2 - 0.33$) and energy scales $\sim 0 - 100$ meV are observed across the phase diagram, at least to $p^\star$. The spin and charge fluctuations show longer correlation lengths and extend to smaller energy scales at lower temperatures. Recent work suggests low-energy scales of ~ 20 meV for charge fluctuations for $0.14 \lesssim p \lesssim 0.19$ (106, 118) and ~ 5 meV for $p = 0.22 \gtrsim p^\star$ for spin fluctuations in LSCO (109). Higher resolution measurements of the charge correlations may clarify this.

Charge order frozen on a much lower frequency scale (25, 31, 32, 21, 51, 11) is observed near $p \approx 1/8$. This order competes with the superconductivity (12, 13). Some theories have predicted that this order arises from 1-$\mathbf{q}$ (uni-directional) stripes made from intertwined charge and spin order. Testing this hypothesis has proved non-trivial because defects can pin or nucleate charge order and the host structure can favor 1-$\mathbf{q}$ order. What is clear is that 1-$\mathbf{q}$ charge order is present in certain structures that favor it (43, 29, 46, 44, 85). These structures break the C_4 symmetry of a single square-lattice CuO_2 plane. In YBCO, the 1-$\mathbf{q}$ order has been observed to lock-in (46) to the the crystal lattice, as is the case for conventional CDWs, when superconductivity is suppressed by a high magnetic field. In $La_{2-x}(Sr,Ba)_x CuO_4$, data is consistent the structure favoring the coupling of a SDW to the CDW leading to 1-$\mathbf{q}$ 'stripe-like' behavior (14, 64, 85, 88, 40). In other materials (e.g. YBCO, Hg1201) data at low field is consistent with a 2-$\mathbf{q}$ structure. Evidence comes from diffraction experiments on detwinned anisotropic materials where two $\mathbf{q}$s are observed (50), real-space STM imaging of the CDW in vortex halos where a 2-$\mathbf{q}$ pattern is observed (16) and quantum oscillations (18, 103, 133). The observed correlation length of the 2-$\mathbf{q}$ order is typically $\xi \lesssim 100$ Å, suggesting that it is limited by pinning to quenched disorder (or vortex halos).

There has been remarkable progress in our understanding of the charge correlations in cuprate superconductors in recent years. However, there are some significant issues to be resolved. Below we summarize the progress discussed in this review and note some issues which require further work.

SUMMARY POINTS

1. CDW "order" near $p = 1/8$ is a universal property of layered cuprates.
2. The microscopic nature of CDW order (correlation length, number of $\mathbf{q}$ components, volume fraction) varies with host structure and the character of disorder.
3. 2-$\mathbf{q}$ 2D order is nucleated by defects and cores of superconducting vortices.
4. 1-$\mathbf{q}$ 3D order occurs in the presence of symmetry breaking perturbation of the host lattice.
5. CDW order competes inhomogeneously with superconductivity.
6. CDW fluctuations are present near $\mathbf{q}_{\mathrm{CDW}}$ and couple strongly to oxygen phonon modes.

FUTURE ISSUES

1. Would 3D charge order exist in all cuprates at $p \sim 1/8$ in the absence of disorder and superconductivity at high magnetic field, and if so, would it be 1-$\mathbf{q}$ or 2-$\mathbf{q}$?
2. What factors determine the distinct $\mathbf{q}_{\mathrm{CDW}}$ for different cuprates?
3. How are spin and charge fluctuations related across the phase diagram?
4. Does CDW order compete with electron pairing or superconducting phase order?

DISCLOSURE STATEMENT

ACKNOWLEDGMENTS

LITERATURE CITED

1. Keimer B, Kivelson SA, Norman MR, Uchida S, Zaanen J. 2015. *Nature* 518(7538):179–186
2. Timusk T, Statt B. 1999. *Reports on Progress in Physics* 62(1):61
3. Fradkin E, Kivelson SA, Tranquada JM. 2015. *Rev. Mod. Phys.* 87:457–482
4. Wilson JA, Di Salvo FJ, Mahajan S. 1975. *Advan. Phys.* 24(2):117–201
5. Monceau P. 2012. *Advan. Phys.* 61(4):325–581
6. Johannes MD, Mazin II. 2008. *Phys. Rev. B* 77(16):165135
7. Ulbrich H, Braden M. 2012. *Physica C: Superconductivity* 481:31–45
8. Comin R, Damascelli A. 2016. *Annu. Rev. Condens. Matter Phys.* 7(1):369–405

9. Dai J, Calleja E, Alldredge J, Zhu X, Li L, et al. 2014. *Phys. Rev. B* 89(16):165140
10. Arguello CJ, Chockalingam SP, Rosenthal EP, Zhao L, Gutiérrez C, et al. 2014. *Phys. Rev. B* 89(23):235115
11. Wu T, Mayaffre H, Krämer S, Horvatić M, Berthier C, et al. 2015. *Nat. Commun.* 6(1):6438
12. Ghiringhelli G, Le Tacon M, Minola M, Blanco-Canosa S, Mazzoli C, et al. 2012. *Science* 337(6096):821–825
13. Chang J, Blackburn E, Holmes AT, Christensen NB, Larsen J, et al. 2012. *Nat. Phys.* 8(12):871–876
14. Tranquada JM, Sternlieb BJ, Axe JD, Nakamura Y, Uchida S. 1995. *Nature* 375(6532):561–563
15. Abbamonte P, Rusydi A, Smadici S, Gu GD, Sawatzky GA, Feng DL. 2005. *Nat. Phys.* 1(3):155–158
16. Hoffman JE, Hudson EW, Lang KM, Madhavan V, Eisaki H, et al. 2002. *Science* 295(5554):466–469
17. Howald C, Eisaki H, Kaneko N, Greven M, Kapitulnik A. 2003. *Phys. Rev. B* 67(1):014533
18. Doiron-Leyraud N, Proust C, LeBoeuf D, Levallois J, Bonnemaison JB, et al. 2007. *Nature* 447(7144):565–568
19. Millis AJ, Norman MR. 2007. *Phys. Rev. B* 76:220503(R)
20. Harrison N, Sebastian SE. 2011. *Phys. Rev. Lett.* 106(22):226402
21. Wu T, Mayaffre H, Krämer S, Horvatić M, Berthier C, et al. 2011. *Nature* 477(7363):191–194
22. Singer PM, Hunt AW, Imai T. 2002. *Phys. Rev. Lett.* 88(4):047602
23. Blanco-Canosa S, Frano A, Schierle E, Porras J, Loew T, et al. 2014. *Phys. Rev. B* 90(5):054513
24. Croft TP, Lester C, Senn MS, Bombardi A, Hayden SM. 2014. *Phys. Rev. B* 89(22):224513
25. Tranquada JM, Gu GD, Hücker M, Jie Q, Kang HJ, et al. 2008. *Phys. Rev. B* 78(17):174529
26. Tabis W, Yu B, Bialo I, Bluschke M, Kolodziej T, et al. 2017. *Phys. Rev. B* 96(13):134510
27. Lee WS, Zhou KJ, Hepting M, Li J, Nag A, et al. 2021. *Nat. Phys.* 17(1):53–57
28. Hamidian MH, Edkins SD, Kim CK, Davis JC, Mackenzie AP, et al. 2016. *Nat. Phys.* 12(2):150–156
29. Chang J, Blackburn E, Ivashko O, Holmes AT, Christensen NB, et al. 2016. *Nat Commun* 7:11494
30. Chen XM, Thampy V, Mazzoli C, Barbour AM, Miao H, et al. 2016. *Phys. Rev. Lett.* 117(16):167001
31. Blackburn E, Chang J, Said AH, Leu BM, Liang R, et al. 2013. *Phys. Rev. B* 88(5):054506
32. Le Tacon M, Bosak A, Souliou SM, Dellea G, Loew T, et al. 2014. *Nat. Phys.* 10(1):52–58
33. Arpaia R, Caprara S, Fumagalli R, Vecchi GD, Peng YY, et al. 2019. *Science* 365(6456):906–910
34. Robertson JA, Kivelson SA, Fradkin E, Fang AC, Kapitulnik A. 2006. *Phys. Rev. B* 74(13):134507
35. Fine BV. 2016. *Science* 351(6270):235–235
36. Hanaguri T, Lupien C, Kohsaka Y, Lee DH, Azuma M, et al. 2004. *Nature* 430(7003):1001–1005
37. Mukhopadhyay S, Sharma R, Kim CK, Edkins SD, Hamidian MH, et al. 2019. *Proc. Natl. Acad. Sci. USA* 116(27):13249–13254
38. v. Zimmermann M, Vigliante A, Niemöller T, Ichikawa N, Frello T, et al. 1998. *Europhys. Lett.* 41(6):629
39. Kim YJ, Gu GD, Gog T, Casa D. 2008. *Phys. Rev. B* 77(6):064520
40. Sears J, Shen Y, Krogstad MJ, Miao H, Bozin ES, et al. 2023. *Phys. Rev. B* 107(11):115125
41. Achkar AJ, Mao X, McMahon C, Sutarto R, He F, et al. 2014. *Phys. Rev. Lett.* 113(10):107002
42. Caplan Y, Orgad D. 2017. *Phys. Rev. Lett.* 119(10):107002
43. Gerber S, Jang H, Nojiri H, Matsuzawa S, Yasumura H, et al. 2015. *Science* 350(6263):949–952
44. Kim HH, Souliou SM, Barber ME, Lefrançois E, Minola M, et al. 2018. *Science* 362(6418):1040–1044

45. Bluschke M, Frano A, Schierle E, Putzky D, Ghorbani F, et al. 2018. *Nat. Commun.* 9(1):2978
46. Vinograd I, Zhou R, Hirata M, Wu T, Mayaffre H, et al. 2021. *Nat. Commun.* 12(1):3274
47. McMillan WL. 1975. *Phys. Rev. B* 12(4):1187–1196
48. Pouget JP. 2016. *Comptes Rendus Physique* 17(3):332–356
49. Caplan Y, Wachtel G, Orgad D. 2015. *Phys. Rev. B* 92(22):224504
50. Blackburn E, Chang J, Hucker M, Holmes AT, Christensen NB, et al. 2013. *Phys. Rev. Lett.* 110(13):137004
51. Wu T, Mayaffre H, Krämer S, Horvatić M, Berthier C, et al. 2013. *Nat. Commun.* 4(1):2113
52. Grissonnanche G, Cyr-Choinière O, Laliberté F, René de Cotret S, Juneau-Fecteau A, et al. 2014. *Nat. Commun.* 5(1):3280
53. Jang H, Lee WS, Nojiri H, Matsuzawa S, Yasumura H, et al. 2016. *Proceedings of the National Academy of Sciences* 113(51):14645–14650
54. Chan MK, Harrison N, McDonald RD, Ramshaw BJ, Modic KA, et al. 2016. *Nat. Commun.* 7(1):12244
55. McMillan WL. 1976. *Phys. Rev. B* 14(4):1496–1502
56. Mesaros A, Fujita K, Edkins SD, Hamidian MH, Eisaki H, et al. 2016. *Proc. Nat. Acad. Sci.* 113(45):12661–12666
57. Chen XM, Mazzoli C, Cao Y, Thampy V, Barbour AM, et al. 2019. *Nat. Commun.* 10(1):1435
58. Fujita M, Goka H, Yamada K, Tranquada JM, Regnault LP. 2004. *Phys. Rev. B* 70(10):104517
59. Hücker M, v. Zimmermann M, Gu GD, Xu ZJ, Wen JS, et al. 2011. *Phys. Rev. B* 83(10):104506
60. Li Q, Hücker M, Gu GD, Tsvelik AM, Tranquada JM. 2007. *Phys. Rev. Lett.* 99:067001
61. Agterberg DF, Davis JCS, Edkins SD, Fradkin E, Van Harlingen DJ, et al. 2020. *Annu. Rev. Condens. Matter Phys.* 11(1):231–270
62. Edkins SD, Kostin A, Fujita K, Mackenzie AP, Eisaki H, et al. 2019. *Science* 364:976–980
63. Christensen NB, Chang J, Larsen J, Fujita M, Oda M, et al. 2014. ArXiv.1404.3192
64. Choi J, Wang Q, Jöhr S, Christensen NB, Küspert J, et al. 2022. *Phys. Rev. Lett.* 128(20):207002
65. Momma K, Izumi F. 2011. *J. Appl/ Cryst.* 44(6):1272
66. Forgan EM, Blackburn E, Holmes AT, Briffa AKR, Chang J, et al. 2015. *Nat. Commun.* 6:10064
67. Fujita K, Hamidian MH, Edkins SD, Kim CK, Kohsaka Y, et al. 2014. *Proc. Nat. Acad. Sci.* 111(30):E3026–E3032
68. Campbell BJ, Stokes HT, Tanner DE, Hatch DM. 2006. *J. App. Crystal.* 39(4):607–614
69. Comin R, Sutarto R, He F, da Silva Neto EH, Chauviere L, et al. 2015. *Nat. Mater.* 14(8):796–800
70. Achkar AJ, He F, Sutarto R, McMahon C, Zwiebler M, et al. 2016. *Nat. Mater.* 15(6):616–620
71. McMahon C, Achkar AJ, da Silva Neto EH, Djianto I, Menard J, et al. 2020. *Sci. Adv.* 6(45):eaay0345
72. Ma Q, Rule KC, Cronkwright ZW, Dragomir M, Mitchell G, et al. 2021. *Phys. Rev. Research* 3(2):023151
73. Gupta NK, McMahon C, Sutarto R, Shi T, Gong R, et al. 2021. *Proc. Natl. Acad. Sci. USA* 118(34)
74. Lee S, Huang EW, Johnson TA, Guo X, Husain AA, et al. 2022. *Proc. Natl. Acad. Sci. USA* 119(15):e2119429119
75. Hücker M, v. Zimmermann M, Gu GD, Xu ZJ, Wen JS, et al. 2011. *Phys. Rev. B* 83:104506
76. Hücker M, Christensen NB, Holmes AT, Blackburn E, Forgan EM, et al. 2014. *Phys. Rev. B* 90(5):054514
77. Dai P, Mook HA, Hunt RD, Dogan F. 2001. *Phys. Rev. B* 63(5):054525
78. Headings NS, Hayden SM, Kulda J, Babu NH, Cardwell DA. 2011. *Phys. Rev. B* 84(10):104513
79. Peng YY, Fumagalli R, Ding Y, Minola M, Caprara S, et al. 2018. *Nat. Mats* 17(8):697–702
80. Enoki M, Fujita M, Nishizaki T, Iikubo S, Singh DK, et al. 2013. *Phys. Rev. Lett.* 110(1):017004

81. Wen JJ, Huang H, Lee SJ, Jang H, Knight J, et al. 2019. *Nat. Commun.* 10(1):3269
82. Miao H, Fabbris G, Koch RJ, Mazzone DG, Nelson CS, et al. 2021. *npj Quant. Mats.* 6(1):31
83. Tam CC, Zhu M, Ayres J, Kummer K, Yakhou-Harris F, et al. 2022. *Nat. Commun.* 13:570
84. Yamada K, Lee CH, Kurahashi K, Wada J, Wakimoto S, et al. 1998. *Phys. Rev. B* 57(10):6165–6172
85. Frison R, Küspert J, Wang Q, Ivashko O, Zimmermann Mv, et al. 2022. *Phys. Rev. B* 105(22):224113
86. Jacobsen H, Zaliznyak IA, Savici AT, Winn BL, Chang S, et al. 2015. *Phys. Rev. B* 92(17):174525
87. Thampy V, Dean MPM, Christensen NB, Steinke L, Islam Z, et al. 2014. *Phys. Rev. B* 90(10):100510(R)
88. Simutis G, Küspert J, Wang Q, Choi J, Bucher D, et al. 2022. *Commun. Phys.* 5(1):296
89. Kohsaka Y, Taylor C, Fujita K, Schmidt A, Lupien C, et al. 2007. *Science* 315(5817):1380–1385
90. Parker CV, Aynajian P, da Silva Neto EH, Pushp A, Ono S, et al. 2010. *Nature* 468(7324):677–680
91. LeBoeuf D, Doiron-Leyraud N, Vignolle B, Sutherland M, Ramshaw BJ, et al. 2011. *Phys. Rev. B* 83(5):054506
92. Allais A, Chowdhury D, Sachdev S. 2014. *Nat. Commun.* 5(1):5771
93. Bel R, Behnia K, Berger H. 2003. *Phys. Rev. Lett.* 91(6):066602
94. Putzke C, Benhabib S, Tabis W, Ayres J, Wang Z, et al. 2021. *Nat. Phys.* 17(7):826–831
95. Bangura AF, Rourke PMC, Benseman TM, Matusiak M, Cooper JR, et al. 2010. *Phys. Rev. B* 82(14):140501(R)
96. Wasserman A, Springford M. 1996. *Advan. Phys.* 45(6):471–503
97. Gannot Y, Ramshaw BJ, Kivelson SA. 2019. *Phys. Rev. B* 100(4):045128
98. Ramshaw BJ, Sebastian SE, McDonald RD, Day J, Tan BS, et al. 2015. *Science* 348(6232):317–320
99. Nakata S, Yang P, Barber ME, Ishida K, Kim HH, et al. 2022. *npj Quant. Mats.* 7(1):118
100. Audouard A, Jaudet C, Vignolles D, Liang R, Bonn DA, et al. 2009. *Phys. Rev. Lett.* 103(15):157003
101. Briffa AKR, Blackburn E, Hayden SM, Yelland EA, Long MW, Forgan EM. 2016. *Phys. Rev. B* 93(9):094502
102. Maharaj AV, Zhang Y, Ramshaw BJ, Kivelson SA. 2016. *Phys. Rev. B* 93(9):094503
103. Barišić N, Badoux S, Chan MK, Dorow C, Tabis W, et al. 2013. *Nat. Phys.* 9(12):761–764
104. Chan MK, McDonald RD, Ramshaw BJ, Betts JB, Shekhter A, et al. 2020. *Proc. Nat. Acad. Sci.* 117(18):9782–9786
105. Nag A, Zhu M, Bejas M, Li J, Robarts HC, et al. 2020. *Phys. Rev. Lett.* 125(25):257002
106. Huang HY, Singh A, Mou CY, Johnston S, Kemper AF, et al. 2021. *Phys Rev X* 11(4):041038
107. Devereaux TP, Shvaika AM, Wu K, Wohlfeld K, Jia CJ, et al. 2016. *Phys. Rev. X* 6(4):041019
108. von Arx K, Wang Q, Mustafi S, Mazzone DG, Horio M, et al. 2023. *npj Quant. Mats.* 8(1):7
109. Zhu M, Voneshen DJ, Raymond S, Lipscombe OJ, Tam CC, Hayden SM. 2023. *Nat. Phys.* 19(1):99–105
110. Husain AA, Mitrano M, Rak MS, Rubeck S, Uchoa B, et al. 2019. *Phys. Rev. X* 9(4):041062
111. Hepting M, Chaix L, Huang EW, Fumagalli R, Peng YY, et al. 2018. *Nature* 563:374–378
112. Giuliani G, Vignale G. 2005. Quantum theory of the electron liquid. CUP
113. Pintschovius L, Reznik D, Reichardt W, Endoh Y, Hiraka H, et al. 2004. *Phys. Rev. B* 69:214506
114. Reznik D, Pintschovius L, Ito M, Iikubo S, Sato M, et al. 2006. *Nature* 440:1170
115. Miao H, Ishikawa D, Heid R, Le Tacon M, Fabbris G, et al. 2018. *Phys. Rev. X* 8(1):011008
116. He Y, Wu S, Song Y, Lee WS, Said AH, et al. 2018. *Phys. Rev. B* 98(3):035102
117. Weber F, Rosenkranz S, Castellan JP, Osborn R, Hott R, et al. 2011. *Phys. Rev. Lett.* 107(10):107403

118. Arpaia R, Martinelli L, Sala MM, Caprara S, Nag A, et al. 2022. arxiv/2208.13918
119. Zaanen J, Gunnarsson O. 1989. *Phys. Rev. B* 40:7391
120. Schulz HJ. 1989. *J. Phys. France* 50(18):2833–2849
121. Machida K. 1989. *Physica C* 158(1):192–196
122. Löw U, Emery VJ, Fabricius K, Kivelson SA. 1994. *Phys. Rev. Lett.* 72(12):1918–1921
123. Fine BV. 2004. *Phys. Rev. B* 70:224508
124. Castellani C, Di Castro C, Grilli M. 1995. *Phys. Rev. Lett.* 75:4650–4653
125. Caprara S, Di Castro C, Seibold G, Grilli M. 2017. *Phys. Rev. B* 95(22):224511
126. White SR, Scalapino DJ. 1998. *Phys. Rev. Lett.* 80:1272–1275
127. Corboz P, Rice TM, Troyer M. 2014. *Phys. Rev. Lett.* 113:046402
128. Huang EW, Mendl CB, Liu S, Johnston S, Jiang HC, et al. 2017. *Science* 358(6367):1161–1164
129. Mai P, Karakuzu S, Balduzzi G, Johnston S, Maier TA. 2022. *Proc. Natl. Acad. Sci. USA* 119(7):e2112806119
130. Arovas DP, Berg E, Kivelson SA, Raghu S. 2022. *Annu. Rev. Condens. Matter Phys.* 13(1):239–274
131. Fujita M, Hiraka H, Matsuda M, Matsuura M, M. Tranquada J, et al. 2012. *J. Phys. Soc. Jpn.* 81(1):011007
132. Krien F, Worm P, Chalupa-Gantner P, Toschi A, Held K. 2022. *Commun. Phys.* 5(1):336
133. Tan BS, Harrison N, Zhu Z, Balakirev F, Ramshaw BJ, et al. 2015. *Proc. Natl. Acad. Sci. U.S.A.* 112(31):9568–9572